



ELSEVIER

Available online at www.sciencedirect.com

SCIENCE @ DIRECT®

Journal of Chromatography A, 1006 (2003) 101–120

JOURNAL OF
CHROMATOGRAPHY A

www.elsevier.com/locate/chroma

Modelling gradient elution of bioactive multicomponent systems in non-linear ion-exchange chromatography

A. Wiesel^a, H. Schmidt-Traub^{a,*}, J. Lenz^b, J. Strube^c

^aDepartment of Chemical Engineering, University of Dortmund, 44221 Dortmund, Germany

^bBayer Health Care, Biotechnology, 42096 Wuppertal, Germany

^cBayer Technology Services, Fluids Processing, 51368 Leverkusen, Germany

Abstract

A theoretical framework for the ion-exchange behaviour of bioactive substances in non-linear ion-exchange chromatography is described. The aim of the study was the creation of a model basis to support a process design for production-scale ion-exchange chromatography. The theory can be applied to a whole variety of biological substances, such as amino acids, polysaccharides, peptides and proteins and either isocratic or gradient elution can be carried out. The influence of the eluent concentration on the ion-exchange as well as on the characteristic charge was considered. Experimental measurements showed a strong non-linear ion-exchange equilibrium with a transition from a Langmuir-type to a sigmoidal isotherm at higher eluent concentrations. Hereby, the compound binds to the surface though it is not ionic. Therefore, the model considered the possibility of ion-exchange as well as adsorption. A simplified distribution of the counter-ions based on the Gouy–Chapman theory with a discrete distribution of the counter-ions was used. The theory was extended by a selectivity in the double layer to allow specific adsorption. Calculations of adsorption–elution cycles showed, in agreement with the experimental observations, the development of non-linear elution profiles with a desorption fronting. As a result, the column loading and the eluent concentration were varied. The effect of contaminants, in this case sodium ions, was investigated and included in the model. Finally, the model was extended to multicomponent systems to investigate the effect of side components on the retention behaviour. The development of the characteristic elution profiles and the effect of the column loading on the separation are discussed. Calculated concentration profiles along the column at discrete time steps were used to reveal the influence of side components and the underlying separation mechanism. The simulations provided a new insight into the phenomena involved in biochromatography and make convenient design concepts at least doubtful as the separation is in this case mainly determined by the loading step and not by the choice of the elution gradient.

© 2003 Elsevier B.V. All rights reserved.

Keywords: Ion-exchange chromatography; Adsorption isotherms; Preparative chromatography; Gradient elution; Non-linear chromatography; Mathematical modelling

1. Introduction

Ion exchange is a well established method in

*Corresponding author. Tel.: +49-231-755-2338; fax: +49-231-755-2341.

E-mail address: schmtr@ct.uni-dortmund.de (H. Schmidt-Traub).

analytical chemistry and the earliest reports date back to 1850 when Thompson studied the adsorption of ammonium ions to soils [1]. Today, ion-exchange is—besides reversed-phase chromatography—the most popular separation method in liquid chromatography. At first ion-exchange was applied to analytical purposes, but during the last few decades it has also

become established as a purification method in preparative or, more precisely, production scale. Especially the demands of mild operation conditions and high purity in combination with high productivity forced the application of chromatographic methods and the development of chromatographic systems. A huge effort has also been made to describe the ion-exchange process theoretically. The literature in this area is vast but the approaches focus on two theories. Helfferich reviews the theories developed before 1960 in his classical book [2]. Of these two the stoichiometric theory has become the most popular, which may result from its simplicity and its familiarity. It is based on the mass action law and describes the retention of a solute ion i as an exchange process with the counter-ion j bound to the surface (overbars represent bound counter-ions). Eq. (1) illustrates this process for monocharged cationic species.



From a physical point of view the main problem of the stoichiometric theory is that it regards only two exchanging ions and neglects activity coefficients of the solute and the counter-ion. These are determined by long-range electrostatical forces, which implies that more than only two ions are involved in the ion-exchange process and therefore cannot be described by a stoichiometric approach. More complex biomacromolecule-like peptides, proteins, etc., even show multipoint interactions due to the distribution of their charges, which interact individually with the fixed charges.

The second theory to describe ion-exchange processes is based on the Donnan potential concept and was introduced by Mattson in his investigation of ion-exchange equilibria in soils [3]. This Donnan potential concept considers counter-ions in two different phases having individual electrostatic potentials. The first attempts to model electrostatic effects started on the basis of this concept but both phases are regarded as homogenous and it does not give any information about how different parameters influence the potential difference between both phases. It is therefore obvious that an application of this approach to ion-exchange chromatography is problematical.

Detailed theories about the interaction between a charged surface and ions in the surrounding electrolyte solution are still active subjects in surface and physical chemistry. In the Gouy–Chapman theory the electrostatical potential in the diffuse double layer is a function of the concentration and the net charge density. It describes non-specific electrostatic interactions and in a simple case the starting point is the Poisson–Boltzmann equation, a second order differential equation making the assumptions of mean field interactions, ions are treated as point charges and the solvent is assumed to possess a constant polarizability. Modifications of this theory include the Stern theory, which takes specific adsorption and the non-zero size of the ions into account. Therefore, the counter-ions are divided into two regions and the so-called Stern layer near the surface is introduced. Between the Stern layer and the outside region—the diffuse part of the layer described by the Poisson–Boltzmann equation—lies the Helmholtz plane, about 2–3 Å from the surface. Cantwell and co-workers used the Stern theory to describe the retention of ions in ion-exchange and ion pair chromatography [4,5]. Their approach considers two contributions to retention of ions: one is the exchange within the diffuse part of the double layer, adsorption on the surface, in their case in the Stern layer, is the other. Considering the highly irregular surfaces used in chromatography, such planes are obviously questionable. Ståhlberg therefore neglected the Stern layer, which means that the Poisson–Boltzmann equation holds up to the surface. Specific adsorption of counter-ions results in changes in the surface charge density, which also influences the electrostatic potential [6]. The potential profile again determines the distribution of solute ions so that the problem must be solved numerically.

The Gouy–Chapman and the Stern theory describe the distribution of counter-ions as a function of the distance from the surface and are based on theoretical investigations of the interaction between a planar surface and solute ions in an electrolyte solution. As mentioned above, one of the major problems of the application of these theories to ion-exchange chromatography is the irregular structure of chromatographic surfaces. Computations carried out by Hasnat and Juvekar even show that typical resin capacities result in inter-site distances, which are too small

for the surrounding water to completely solvate the fixed sites [7]. As a consequence they expect the extent of dissociation of the counter-ions to be less than 10%.

As a result, the adsorption behaviour often shows non-ideal behaviour that cannot be described by constant selectivity coefficients [2]. Myers and Byington explain the non-ideal adsorption behaviour in terms of the energetic heterogeneity of the functional groups of the ion exchanger [8]. In particular, Myers and Byington considered a binomial distribution of the adsorption energies with three adjustable parameters for each binary system, the average adsorption energy, the energy distribution and the skewness of the energy distribution. Thereby, each adsorption site behaves ideally. The model was successfully applied to describe binary and multicomponent adsorption equilibria of amino acids [9,10] and also to describe the uptake equilibria of dipeptides on cation exchange resins [11]. Melis et al. acknowledged the heterogeneity of adsorption sites like in the Myers and Byington model and introduced the idea of a heterogeneous solid into the framework of an equilibrium model based on the mass action law [12]. The heterogeneity of the adsorption sites is given by the average value of the standard free-energy change of the ion-exchange process, a standard deviation for each binary system and one parameter representing the fraction of functional groups of each type. More recently, Melis et al. used this approach to model selectivity reversals in the ion-exchange of amino acids [13].

Whereas amino acids reveal dipole character, the application of ion-exchange to separate molecules with larger three-dimensional charge distribution, e.g. peptides and proteins, raises new questions. The solute ions often have complex chemical structures. Their charge is a function of the pH and distribution along the surface and their dimension is of the same order as the double layer itself, which is usually thought to extend up to 30 Å from the surface [14]. The assumption of point charges is not valid for complex molecular structures. For that reason one of the first questions is which molecules are able to bind to the surface at all.

Amino acids show amphoteric behaviour and possess at least two centers that can carry charges. Their actual form as basics, neutrals or acids depends

on the pH value. Yu and Wang described the equilibrium uptake of neutral, basic and acidic amino acids quantitatively and concluded that the uptake is strongly reduced if the negatively charged $-\text{COO}^-$ on the amino acid is present, either in ionic or zwitterionic state [15]. The charge of amino acids is given by the pK values, which are reported to be in the range 1.80–2.95 for the carboxyl group and 8.84–10.78 for the amino group [16]. Therefore, for low ionic strengths, it is proposed that only cationic amino acids can take part in ion-exchange as other species are excluded from the resin phase due to the Donnan effect. Non-ionic interactions, such as hydrophobic properties of the support, are assumed to be of minor importance for retention at the given conditions as their contribution increases at salt concentrations higher than used in this study [17].

Proteins and peptides show a charge distribution along their surface. As a consequence, there may be specific areas on the surface with accumulated charges. In this case they may bind to the surface though their net charge is of the same sign as the functional groups, which usually results in co-ion exclusion. Roth and Lenhoff developed a model to predict protein-surface equilibrium constants based on protein structures and surface properties [18]. In this case the numerical effort is high and calculations of the electrostatic and Van der Waals energies of interaction are very time-intensive. Therefore, simplified descriptions are still state of the art and usually the protein parameters are the size and net charge, while the stationary phase properties are reduced to the surface charge density and the short-range interaction energy [19].

Cramer and Brooks developed a macroscopic model of the charge distribution and size of proteins [20]. Their steric mass action (SMA) model included, besides the equilibrium constant, two coefficients, a stoichiometric and a steric factor. The stoichiometric coefficient is a statistical value and varies with the orientation of the protein with respect to the surface. Bouhallab investigated the same phenomenon resulting in non-integer stoichiometric coefficients for small peptides [21].

In the ion-exchange of peptides, proteins, etc., the size of the molecules usually results in reduced maximal capacities. Cramer and Brooks described this with a shielding of functional groups by ad-

sorbed proteins and introduced a steric coefficient [20]. As a result, the proteins are homogeneously distributed inside the resin phase and size exclusion due to pore size distribution was not considered.

As pointed out previously, there are numerous influences on the adsorption and ion-exchange step itself, respectively, of complex molecules. The application of a model to predict the retention behaviour in non-linear ion-exchange chromatography includes a characterisation of the extra column effects like plant dead volumes, the resin phase including surface properties and the physical properties of the investigated compounds. In gradient elution mode there is a local change of the solvent elution strength so that the influence of the solvent on the properties of the adsorbent and the compounds has to be considered as well.

In this paper, as a generic example, the retention behaviour of a bioactive compound in ion-exchange chromatography in the presence of eluent ions is discussed. The active centre of the compound is given by a secondary amine so that it can act in neutral or cationic form. The protonation, electro-neutrality and the influence of the eluent ion concentration on the ion-exchange equilibrium were considered. Model parameters were determined experimentally and by least squares fitting. Subsequently, the model was validated in adsorption–elution cycles with varying column loadings and eluent strength. Model extensions include the influence of contaminants, such as salt ions, as well as side components on the retention.

2. Theory

2.1. Protonation equilibrium in aqueous solution

The compound investigated in this study interacts with the surface via a secondary amine group. Therefore, its current form is determined by the solution pH and, in particular, we have:



which leads to an excess of the cationic form at low values of the solution pH.

Knowing the total concentration of compound P

and assuming ideal behaviour for the aqueous phase, the concentration of the cationic form can be calculated as follows:

$$c_{PH^+} = \frac{c_{P,\text{total}}}{1 + \frac{1}{K_p c_{H^+}}} \quad (3)$$

where K_p is the equilibrium constant of the protonation reaction [see Eq. (2)]. The concentration of the neutral form can be calculated easily by summing up the individual concentrations:

$$c_{P,\text{total}} = c_P + c_{PH^+} \quad (4)$$

The role of side components is discussed later but based on their molecular structure it is assumed that the same interactions and mathematical descriptions as for compound P can be applied. The dissociation of water is given by the ionic product of water K_w . Other considered compounds are HCl as eluent and NaCl as salt. Complete dissociation is assumed for strong electrolytes, such as HCl and NaCl. The concentration of chloride ions in solution is given by the feed concentrations of salt and eluent:

$$c_{Cl^-} = c_{HCl} + c_{NaCl} \quad (5)$$

The concentrations of all species in solution can be computed from Eqs. 3–5 once the concentration of the hydrogen ion is known. The solution pH can be measured or calculated through the local electro-neutrality condition:

$$c_{PH^+} + c_{H^+} + c_{Na^+} = c_{Cl^-} + c_{OH^-} \quad (6)$$

2.2. Column modelling and mass transfer

Numerous models are available to simulate the development of band profiles in fixed beds [22]. The axial dispersion model with uniformly sized spherical beads has proven to be useful to describe the mobile phase in liquid chromatography:

$$\frac{\partial c_i^0}{\partial t} = -u \frac{\partial c_i^0}{\partial x} + D_{ax} \frac{\partial^2 c_i^0}{\partial x^2} + \frac{6}{d_p} \frac{(1-\varepsilon)}{\varepsilon} \varepsilon_p \sum J_{i+1/0/-} \Big|_{r=R_p} \quad (7)$$

where c_i^0 is the concentration of component i in the mobile phase, u is the interstitial fluid velocity and ε

is the bed voidage. This equation considers convective mass transfer, axial dispersion and mass transfer between the two phases at the particle surface. The axial dispersion coefficient is estimated using the correlation by Chung and Wen [23].

At the column inlet and outlet Danckwerts' boundary conditions were used:

$$x = 0; \quad uc_{i,\text{Feed}} = uc_i^0 - D_{\text{ax}} \frac{\partial c_i^0}{\partial x} \quad (8)$$

$$x = L; \quad \frac{\partial c_i^0}{\partial x} = 0 \quad (9)$$

The mass balance PDE (partial differential equation) Eq. (7) is applied to the total concentrations of compound P, the side components, sodium and chloride ions. All other species involved in the ion-exchange process are calculated using Eqs. 3–6. For that reason the sum of contributing species (cationic and neutral for compound P, anionic for chloride ions) represents the total mass transfer term, given by $\sum J_{i+/0/-}$, as the diffusion fluxes of both forms of compound P are considered individually.

The concentration profile inside the particle is calculated by application of a finite-difference scheme in spherical coordinates to the mass balance PDE, which is given by:

$$\frac{\partial c_i^i}{\partial t} + \left(\frac{1 - \varepsilon_p}{\varepsilon_p} \right) \frac{\partial q_i}{\partial t} = - \frac{1}{r^2} \frac{\partial}{\partial r} \left(r^2 \sum J_{i+/0/-} \right) \quad (10)$$

where c_i^i is the concentration of component i in the pores of the macroporous resin phase, and q_i is the amount adsorbed on the surface, respectively, bound inside the double layer. The particle porosity ε_p in Eq. (10) is introduced to consider the appropriate volume fractions.

Inside the particle the same balancing method as in the bulk solution is used. Eq. (10) is applied to the total concentrations of compound P, the side components, sodium and chloride ions. Furthermore, compound P underlies the same protonation equilibrium as a function of the total concentration and the concentration of hydrogen ions in the stagnant liquid inside the pores. All other species involved in the ion-exchange process are calculated using Eqs. 3–6.

The external film resistance is assumed to be of minor importance in a lumped mass transfer coefficient

dominated by intraparticle diffusion. Therefore, the boundary condition is given by the equality of the concentration at the particle surface and in the bulk solution. A symmetrical concentration profile inside the particle results in the concentration gradient set to zero at the centre of the particle.

$$r = R_p; \quad c_i^i \Big|_{r=R_p} = c_i^0 \quad (11)$$

$$r = 0; \quad \frac{\partial c_i^i}{\partial r} = 0 \quad (12)$$

Mass transfer kinetics are considered as hindered diffusion in a radial direction from the surface to the middle of the particle. However, as ion-exchange processes usually are not limited by adsorption kinetics, at a given position inside the particle, local equilibrium is assumed between ions in solution and ions on functional groups [24].

Due to the macroporous resin structure the mass transfer is based only on pore diffusion and surface diffusion is assumed to be of minor importance and is neglected. The Nernst–Planck equation for pore diffusion is used to take the influence of the charge of the solute ions on the mass transfer into account [25].

$$J_i = - \mathbf{D}_i \left[\frac{\partial c_i^i}{\partial r} + z_i c_i^i \frac{F}{RT} \frac{\partial \phi}{\partial r} \right] \quad (13)$$

where \mathbf{D}_i is the diffusivity of component i in the stagnant liquid phase inside the particle, F is the Faraday constant, R the ideal gas constant, T the temperature and ϕ the electrical potential caused by the different mobilities of diffusing ions. Individual fluxes in multicomponent systems are calculated by substituting the electrical potential ϕ by the electroneutrality and zero-current condition, which means that the sum of fluxes across a border multiplied with the charge must be zero. This method was proposed by Hwang et al. [26].

The values of the diffusivities of hydrogen and chloride ions are reported to be $9.31 \times 10^{-9} \text{ m}^2/\text{s}$ for hydrogen, $1.33 \times 10^{-9} \text{ m}^2/\text{s}$ for sodium and $2.03 \times 10^{-9} \text{ m}^2/\text{s}$ for chloride [27], while the diffusivity for compound P is estimated through the correlation by Polson [28]. Both forms, ionic and neutral, are assumed to have the same diffusivity, as proposed by Kim et al. [29]. The difference in diffusion fluxes is

due to the additional driving force on the ionic form because of the electrostatical potential gradient. A tortuosity factor τ is introduced to take the effective lengths of the pores into account and is equal to 1 for a cylindrical pore. Satterfield recommends a value of τ between 2 and 6 when surface diffusion is negligible [30]. The effective diffusivity in the pores is given by:

$$\mathbf{D}_i = \frac{D_i}{\tau} \quad (14)$$

The porosity is already considered in Eq. (10). This tortuosity factor is determined in a one-time pulse experiment with compound P. As mentioned above, the diffusivity of compound P in free solution is based on the correlation by Polson [28].

2.3. Double layer

As stated above, the interaction between the fixed charges on the surface and ions in the surrounding electrolyte solution cannot be seen as a stoichiometric 1:1 complex. The negatively charged groups are chemically bound to the surface and at least partially dissociated. They create an electrostatical potential difference between the surface and the ionic bulk solution. The concentration of counter-ions is a function of the distance from the oppositely charged fixed charges and a result of the electrostatical interaction. As the counter-ions “shield” each other and due to entropic effects the concentration decreases from the surface to the bulk solution. Described in thermodynamic terms, the concentration profile is a result of the condition that the electrochemical potential must be equal at every point.

The extension of the double layer and the resulting concentration profile is calculated by the method proposed by Ståhlberg [6]. At first the Gouy–Chapman theory (for a symmetrical 1:1 electrolyte) was applied on the condition that the Poisson–Boltzmann equation holds from the bulk, respectively, core of the pore up to the surface. The Poisson–Boltzmann equation is described by Eq. (15), where ρ is the charge density at a point located a distance x from the surface [31].

$$\frac{d^2}{dx^2}\psi(x) = -\frac{\rho(x)}{\varepsilon_0\varepsilon_r} \quad (15)$$

The thermodynamic equilibrium requires that the electrochemical potential is equal at every point. So the potential at a distance x from the surface is given by:

$$\mu_i(x) = \mu_{i0} + RT \ln X_i(x) + z_i F \psi(x) \quad (16)$$

where $X_i(x)$ is the mole fraction of component i at point x . The potential profile can be obtained by calculating the surface charge density, which is a function of the bulk concentration c_i and the difference in the electrostatical potential between the surface and the bulk solution:

$$\sigma = \sqrt{8RTc_i^i\varepsilon_0\varepsilon_r} \sinh(z_i F \psi_0 / RT) \quad (17)$$

and solving Eq. (17) for the electrostatical potential

$$\psi_0 = \frac{2RT}{z_i F} \ln \left(\frac{\sigma}{\sqrt{8\varepsilon_0\varepsilon_r RT c_i^i}} + \left(\frac{\sigma^2}{8\varepsilon_0\varepsilon_r RT c_i^i} + 1 \right)^{1/2} \right) \quad (18)$$

The electrostatical potential in a point located a distance x from a surface is

$$\psi(x) = \frac{2RT}{F} \ln \left(\frac{1 + \gamma \exp(-\kappa x)}{1 - \gamma \exp(-\kappa x)} \right) \quad (19)$$

with

$$\gamma = \tanh(F\psi_0/4RT) \quad (20)$$

and the reciprocal value of the Debye length $1/\kappa$

$$\kappa = F \left(\frac{2z_i^2 c_i}{\varepsilon_0 \varepsilon_r RT} \right)^{1/2} \quad (21)$$

From Eq. (16) one obtains the concentration profile in the diffuse part of the double layer based on the bulk concentration:

$$c_i(x) = c_i \exp(-z_i F \psi(x) / RT) \quad (22)$$

Fig. 1 shows calculations of the counter-ion concentration profiles for three different concentrations as a function of the distance based on the Gouy–Chapman theory. Assumptions are a planar surface with constant surface charge density and a 1:1 electrolyte. The higher the bulk concentration the shorter the diffuse layer as the electrostatical potential diminishes faster with increasing charge den-

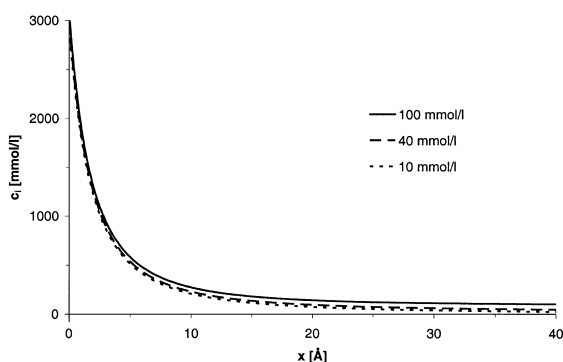


Fig. 1. Counter-ion concentration as a function of the distance from the surface for different bulk concentrations of a 1:1 electrolyte at 10, 40 and 100 mmol/l; ϵ_r set to 80 and a constant surface charge density of -0.1 C/m^2 .

sity [see Eq. (15)]. The length of the diffuse layer is about 30–40 Å and of the same order of magnitude as reported by Wesseling and Krishna [14].

2.4. Adsorption and ion-exchange equilibrium

In this paper the concentration profile of counterions is approximated by means of a discrete distribution with two types of functional groups (see Fig. 2). Furthermore, it is assumed that co-ions are completely excluded from the double layer. The sum of both groups is given by the total exchange capacity of the resin.

$$q_{\text{total}} = q_{\text{total}}^d + q_{\text{total}}^s \quad (23)$$

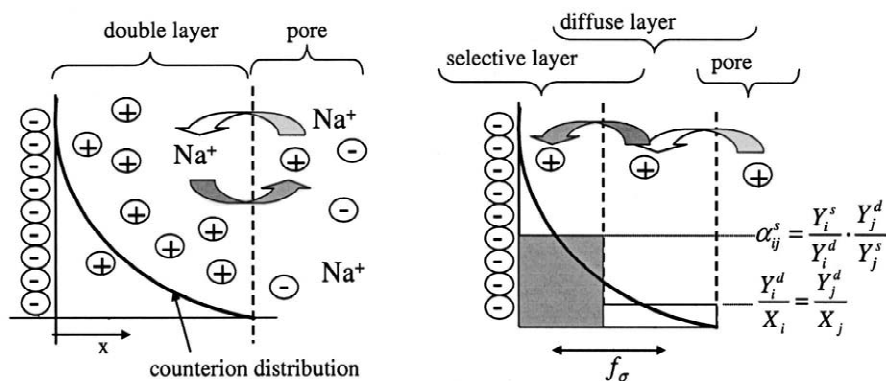
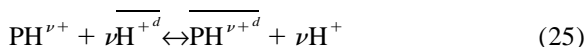


Fig. 2. (a) Distribution of counter-ion concentrations in the diffuse layer following the Gouy–Chapman theory. (b) The mole fractions of ionic compounds in the diffuse layer are assumed to be the same as in the stagnant liquid phase.

The distribution factor of the functional groups f_σ is assigned to the ion-exchange resin and equal for all components. It is determined by parameter estimation routines based on the experimental ion-exchange equilibrium data.

$$q_{\text{total}}^d = f_\sigma q_{\text{total}} \quad (24)$$

The assignment of specific adsorption, steric hindrance, etc., is based on the concentration profile, which is initially guessed using the method proposed by Ståhlberg [6]. The first group, q^d , is close to the pores and represents the part inside the double layer with low counter-ion concentrations (see Fig. 1). The stoichiometric ion-exchange between the diffuse layer and the pore is given by (overbars represent ions in the double layer):



In this study only monovalent ions were exchanged and, therefore, stoichiometric coefficients are not explicitly mentioned below. However, this is not a limitation of the theory. It can be easily applied to different systems [see Eq. (25)].

Based on the calculation of the concentration profile above within the diffuse layer compound P is assumed to be located that far away from the surface that the interaction can be interpreted as that of a charged surface and a point charge. As a result of this the interaction is non-specific, steric effects are negligible and the ions in the diffuse layer are in

equilibrium with the surrounding electrolyte solution. Due to the non-specific binding the mole fraction of counter-ions in the diffuse layer, Y_i^d is the same as in the pores, X_i . In the stoichiometric theory this is identical with a selectivity of one in the diffuse layer α_{ij}^d between two ions i and j .

$$\alpha_{ij}^d = 1 = \frac{q_i^d c_j^i}{c_i^i q_j^d} = \frac{Y_i^d X_j^i}{X_i^i Y_j^d} \quad (26)$$

Eq. (26) describes the retention of counter-ions by transferring an ion from the pore to the diffuse layer. Based on the Donnan potential concept, co-ions are excluded from the double layer. The same is applied to zwitterionic forms, such as amino acids to allow the so-called group separation of amino acids observed by Yu and Wang [15].

However, non-ionic components like the neutral form of compound P can enter the diffuse layer without resistance. For that reason, in the diffuse layer the following reaction of P with bound hydrogen ions is possible:



Hereby, the same equilibrium constant of the protonation reaction K_p as in the bulk solution is used [see Eq. (3)]. As a result of the electroneutrality condition PH^+ is bound to the double layer. In this paper this reaction is defined as adsorption as no counter-ion is transferred from the double layer to the bulk solution.

The second group of the double layer, the so-called selective layer, is located between the diffuse layer and the resin surface. Ions bound in this layer are—besides the electrostatical interaction due to their charge—strongly influenced by their characteristics, i.e. size, charge distribution, multipoint interaction and further non-idealities. Fig. 3 shows one non-ideality in the form of a steric hindrance while accessing the selective layer. These effects are lumped into three specific parameters, the stoichiometric coefficient, a steric factor and a selectivity factor. This layer represents the highly concentrated part of the counter-ion profile calculated before and shown in Fig. 1. Application of the stoichiometric theory to the ion-exchange is defined by the selectivity between the selective and the diffuse layer:

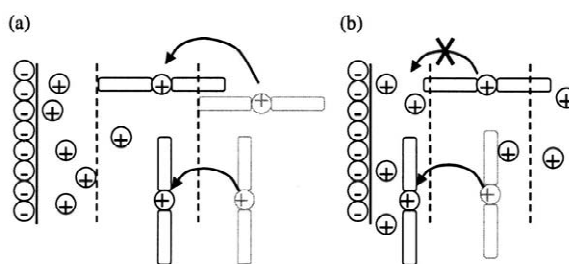


Fig. 3. Schematic illustration of steric hindrance while accessing the functional groups of the selective from the diffuse layer.

$$\alpha_{ij}^s = \frac{q_i^s q_j^d}{q_i^d q_j^s} = \frac{Y_i^s Y_j^d}{Y_i^d Y_j^s} \quad (28)$$

Within the diffuse layer the concentrations are only slightly higher than in the electrolyte solution. This can still be regarded as a diluted solution and therefore a shielding of functional groups due to bound ions of compound P is not realistic. As a result the balance for all functional groups assigned to the diffuse layer is given by:

$$q_{\text{total}}^d = f_{\sigma} q_{\text{tot}} = \sum_n \nu_n q_n^d \quad (29)$$

with ν as the stoichiometric coefficient. However, in the selective layer a steric factor σ is introduced as proposed by Cramer for the ion-exchange of proteins. This coefficient includes the restricted accessibility of the functional groups as well as other effects, such as the limited possibility for solute molecules to solvate the compounds near the surface at high concentrations of that species. The balance for the selective layer is given by:

$$q_{\text{total}}^s = (1 - f_{\sigma}) q_{\text{tot}} = \sum_n (\nu_n + \sigma_n) q_n^s \quad (30)$$

From Eq. (30) the specific capacity is obtained by dividing the total exchange capacity by the sum of the stoichiometric and the steric coefficient.

Interactions of compound P with possible side components are the competitive protonation with hydrogen ions and competition for the adsorption and ion-exchange in the double layer, respectively.

Contaminants like salt ions interact with the components via competitive ion-exchange.

3. Experimental

The resin used in this work, Lewatit (Bayer), is a strong acid macroporous cation exchanger. It is constituted of a polymer backbone based on a styrene–divinylbenzene copolymer with 8% degree of cross-linking. Ion exchange activity of the resin is obtained by sulfonation. The total ion-exchange capacity of the resin, q_{total} , in a packed bed column is given by the manufacturer as 1 mol/l and experimentally verified by transferring the resin from its original hydrogen form to sodium using sodium chloride. The investigated compound P is a pharmaceutical test substance provided by Bayer. Depending on the pH it shows basic character and exists in two forms, neutral and cationic. The protonation constant is measured by titration with hydrochloric acid. HPLC-grade sodium chloride and hydrochloric acid were purchased from Sigma–Aldrich (Steinheim, Germany). The HPLC systems used in this study were a HP1100 (Agilent), an ÄKTAexplorer (Amersham-biosciences) and a Varian HPLC-system. Water was distilled and deionised in a Milli-Q system (Millipore).

All experiments were carried out at room temperature (about 20 °C). The uptake equilibrium of compound P was measured in finite bath experiments in three series; at neutral pH and for two different concentrations of hydrochloric acid. A sample of resin in hydrogen form was contacted with a sample of solution. The density of the wet resin was measured as equal to 0.985 g/cm³. The flasks were shaken for 24 h, which was sufficient time to obtain equilibrium. After a further 3 h of settling the supernatant solute concentration was determined using an analytical HPLC.

A glass column with 2 cm I.D. and a packed bed 20 cm in height was used for breakthrough experiments and to carry out single component adsorption–elution cycles. The breakthrough with a feed concentration that was known to result in saturation of the resin was used to measure the specific capacity. Because of the slow mass transfer kinetics and limited available substance, breakthrough experi-

ments were not applied to measure the uptake equilibrium. Initial conditions for all column experiments were set by regeneration of the resin with 1 M hydrochloric acid followed by intensive washing with water of neutral pH.

Tracer experiments gave the bed voidage (Dextran Blue) and the particle porosity (hydrochloric acid) resulting in a bed voidage equal to 0.36 and a particle porosity of 0.52. In further tracer experiments without column the plant dead volume and the extra-volume between delivery system and the column were determined.

The adsorption–elution cycles were carried out to check the validity of the model and to show the ability to predict elution times and peak shapes. As a result, the column was loaded with the compound at neutral pH; two different loadings were investigated during this study. A washing step followed to elute non-adsorbing solutes. Then, a one-step elution was achieved by switching the input valve. Two different elution solutions were used, hydrochloric acid with a concentration of 10 or 40 mM. After each run the column was regenerated using the procedure described above.

The ion-exchange equilibrium of sodium ions with respect to salt was measured in finite bath experiments. In this case small samples of dried resin were contacted with samples of solution. Sodium chloride was added and the flasks were shaken for 24 h to obtain equilibrium. After that, the concentration of hydrogen and chloride ions in the supernatant solute were determined by titration using NaOH for titration of the free hydrogen ions. The concentration of chloride ions was used by potentiometric titration with AgNO₃.

Multicomponent experiments were carried out in a glass column with 5 cm I.D. The individual concentrations of all components involved were measured after collecting fractions by means of an analytical HPLC system. The same column configuration was used to examine the influence of sodium ions on the retention of the main component. After a rinsing step, a three-step elution each having constant concentrations of hydrochloric acid (10, 20 and 30 mM) was applied to elute the components.

Pulse experiments with constant eluent concentration of 40 mM hydrochloric acid were used to measure the separation factors and the selectivities of

the side components, respectively, with respect to the main compound P based on the retention volume. The tortuosity factor was obtained from these pulse experiments by means of the Aspen Custom Modeler Estimation routine, based on a least squares non-linear solver.

4. Results and discussion

4.1. Ion-exchange equilibrium

The binary ion-exchange equilibrium of compound P with respect to the counter-ion hydrogen was the focus of the experimental part of this study. It is of special importance for this study as the dependency of the ion-exchange equilibrium on the product as well as the eluent concentration directly results in the shape of the peaks in dynamic experiments.

Fig. 4 shows the measured (markers) and calculated (solid lines) ion-exchange equilibria for the three different eluent concentrations. The so-called group separation of amino acids as basics, neutrals and acids described by Melis et al. [13] is not observed in this case. On the contrary, maximum

concentrations in the solid phase were achieved at neutral pH and the isotherm is of nearly rectangular shape. At neutral pH the equilibrium of the protonation reaction [see Eq. (2)], is almost completely on the side of the neutral form of compound P. This behaviour differs from experiments carried out with amino acids, which are not retained in ion-exchange chromatography if not in ionic form. As mentioned above, this behaviour is usually explained with the Donnan potential concept and the co-ion exclusion from the resin phase. In macroporous resins this corresponds with the exclusion from the double layer.

By increasing the concentration of HCl in the feed solution a transition from a Langmuir-type isotherm with a steep gradient at low concentrations to a sigmoidal isotherm can be observed. Thereby, the slope at low product concentrations decreases with increased HCl concentrations. At higher product concentrations the isotherm is bent upwards until the specific capacity limits the resin loading. At lower pH values the cationic fraction of compound P is decreased as the concentration of free hydrogen ions remains high. Compound P acts like a buffer, which causes the sigmoidal shape of the isotherm. This

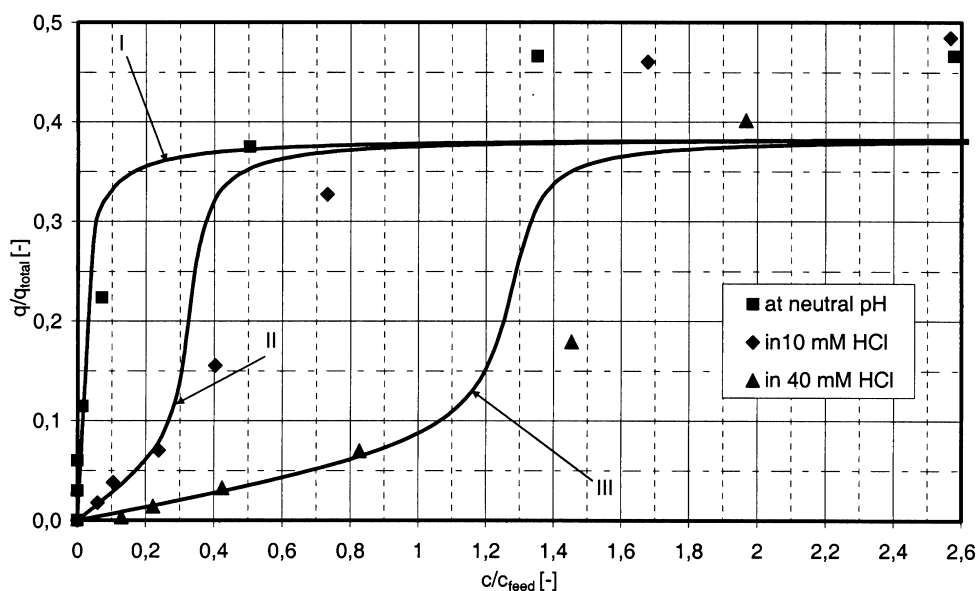


Fig. 4. Experimental (markers) and calculated (solid lines) isotherms displayed as solid-phase concentration versus mobile phase concentration (based on feed concentration in adsorption–elution cycles); I at neutral pH; II in 10 mM HCl solution; III in 40 mM HCl solution.

reflects the ionic fraction of PH^+ with respect to the free hydrogen ions.

The calculated ion-exchange equilibrium obtained by numerical solution of Eqs. 3–6 and Eqs. 23–30 is in satisfactory agreement with the experimental data and the characteristic adsorption behaviour is represented well. This supports the proposed model and especially the idea to allow the adsorption of neutral components, which are not excluded from the resin phase by diffusion into the diffuse layer and the interaction with bound hydrogen ions to bind to the surface.

At high feed concentrations the simulations obviously deviate from the batch experiments, which predict solid-phase concentrations about 20% lower than observed in experiments. This deviation results from the different methods in batch and column experiments. The breakthrough curves in a packed column give maximum specific capacities that are lower than the solid-phase concentrations in batch experiments. This might be due to resin swelling in batch experiments, which affects the number of accessible functional groups. For that reason it is only possible to represent the experimental results at high feed concentrations for either finite batch or column experiments. As the simulations shall be applied to predict column experiments the value obtained from breakthrough experiments is used as the model parameter for the maximum resin loading.

The steric factor can be calculated directly from the total and the specific capacity. Additional model parameters, the double layer distribution factor and the selectivity of compound P, are fitted to the ion-exchange equilibrium data. Table 1 lists the values of the equilibrium model parameters. It is obvious that the compound has a very small affinity to the resin compared with hydrogen ions.

The double layer distribution factor obtained was 0.076, which means that 7.6% of all counter-ions in

the double layer are assigned to the diffuse layer. This value agrees with the estimation by Hasnat and Juvekar who proposed that less than 10% of the counter-ions can be completely solvated [8]. The integration of the counter-ion profile shown in Fig. 1 from the core pore to the surface results in a boundary between diffuse and selective layer about 20 Å away from the surface. Compared to the size of the compound and considering the concentration at that point the conditions applied to the diffuse layer seem to be fulfilled.

4.2. Adsorption–elution cycles

The reliability of the model is shown by comparisons of experimental and theoretically predicted elution profiles. Therefore, four different adsorption–elution cycles are carried out that vary in column loading, based on the specific capacity in percent, and elution strength. The experiments consist of three steps. First the column is loaded with compound P at neutral pH followed by a washing step with water. Finally, elution is achieved by switching the column inlet to either 10 or 40 mmol/l HCl as a one-step elution. The operating conditions are reported in Table 2.

Fig. 5 shows the obtained concentration profiles with respect to dimensionless time. The latter is based on the dead volume time t_0 of unretained small molecules. The dimensionless concentration is based on the feed concentration. The profiles for high column loadings (runs I and II) show a desorption fronting and a stronger diluted adsorption front. The combination of high column loading and high elution strength results in a peak maximum concentration exceeding the feed concentration. This behaviour shows the possibility to use gradient elution chromatography to upgrade dilute solutions.

At lower column loadings the profiles resemble linear chromatography with a Gaussian profile but the same tendencies can be seen at low elution

Table 1
Equilibrium model parameters for compound P

Parameter	Value
Selectivity of compound P	0.01
Double layer distribution factor f_{σ}	0.076
Stoichiometric coefficient	1
Steric factor	2.0

Table 2
Operating conditions in adsorption–elution cycles

Run	I	II	III	IV
Column loading	~40%	~40%	~7%	~7%
Eluent (mmol/l)	40	10	40	10

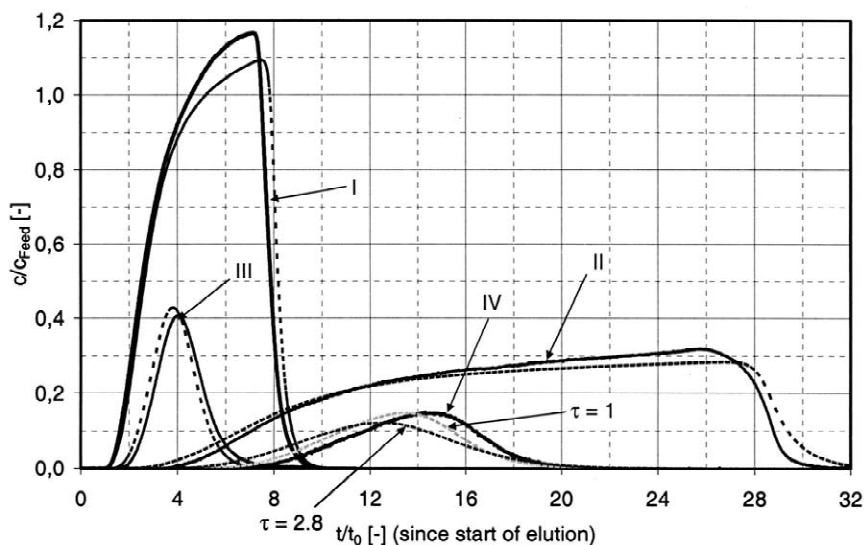


Fig. 5. Comparison between experimental data (solid lines) and simulation results (dotted lines). For low column loadings and low elution strength the influence of mass transfer kinetics on the elution profile is shown by varying the tortuosity coefficient between $\tau=2.8$ (dashed black line) and $\tau=1$ (dashed grey line).

strengths (run IV). This behaviour can be explained by looking at the measured equilibrium in Fig. 4 once again. Starting from the maximum resin phase concentration during the loading step a change to the equilibrium along the isotherms in hydrochloric acid at the column inlet is performed. This causes high concentrations in the aqueous phase due to desorption. At high elution strength the ion-exchange equilibrium shows a nearly linear dependence over a wide concentration range. With small samples injected to the column the solvent change between adsorption step and elution is compensated for rather quickly. So this case approaches normal elution chromatography with decreasing column loading. For high column loadings or low elution concentrations there remains a strong non-linearity and the repeated adsorption in the former unloaded part of the column dilutes the adsorption front.

Fig. 5 shows that the agreement of experimental data and model predictions is satisfactory especially for high elution concentrations with a slight difference in retention observed for low loading (run III). The shapes of the peaks are well represented by the model. The tortuosity factor obtained for the simulations was 2.8 from a parameter estimation using isocratic pulses of compound P in 40 mM hydrochloric

acid and is consistent with the recommendations by Satterfield [30]. However, hindered diffusion has a strong effect on the profile for low column loading and low elution concentration (run IV). In all other cases mass transfer kinetics do not influence the retention time but the steepness of adsorption and desorption fronts. In case IV, as shown in Fig. 5, the profile form changes significantly and the calculated profile with a tortuosity of 1 represents the experimental data much better. It is assumed that this behaviour at low concentrations is due to the diffusivity hindrance that gradually increases with the concentration. However, the theoretically predicted profiles are far within the reproducibility of the experiments.

4.3. Influence of inorganic ions on the retention behaviour

Purification steps using ion-exchange chromatography of pharmaceutical substances are usually accompanied by inorganic contaminants, such as salts from the fermentation broth. The influence of salt ions, represented by sodium chloride, on the retention were investigated.

At first the specific selectivity is fitted to the

ion-exchange equilibrium data shown in Fig. 6. The authors would like to point out that the aim of this section is whether hydrogen or sodium ions bind stronger to the ion-exchange resin. For that reason only a limited number of experiments were performed. The obtained values are listed in Table 3. Usually the resin capacity is measured by transferring the resin from hydrogen to sodium. Therefore, the steric factor is set to zero.

Changes in the ionic strength of the solution as well as salting in and salting out which might influence molecules like proteins does not occur. Therefore, in this paper the influence of salt ions is limited to competition for the fixed charges. Fig. 7 shows the influence of sodium ions on the elution profile of compound P. The experiments are carried out in a column with 5 cm I.D. and a three-step elution (10, 20 and 30 mM HCl) is applied. The presence of sodium ions (a salt concentration of 0.85

Table 3
Equilibrium model parameters for sodium

Parameter	Value
Selectivity with respect to hydrogen	1.3
Double layer distribution factor f_σ	0.076
Stoichiometric coefficient	1
Steric factor	0

g/l is used) evokes a shift of the whole profile to shorter retention times. However, the influence on the adsorption front in terms of time is bigger than that on the peak maximum.

Fig. 8 shows the predicted elution profiles that agree well with the experimental profiles. The sodium ions displace the other components because of the higher selectivity. As a result the effective column length where compound P is able to bind to the surface is decreased and therefore the retention time is smaller. However, this does not explain the

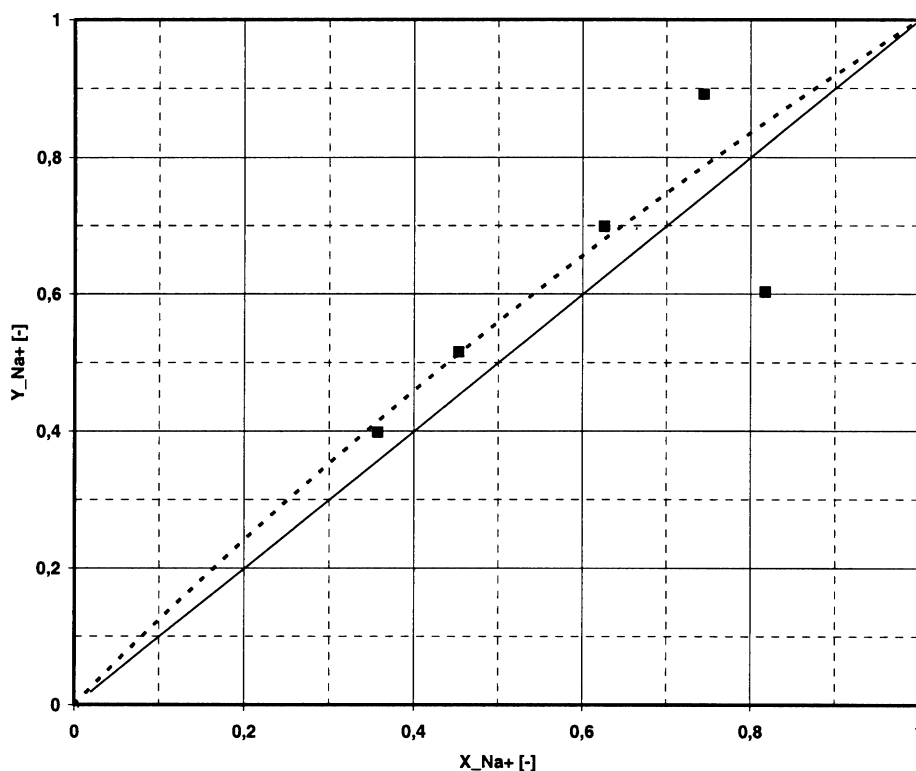


Fig. 6. Ion exchange equilibrium for the system Na^+/H^+ in terms of resin phase ionic fraction, Y, versus the ionic fraction in the aqueous phase, X, of sodium ion with respect to hydrogen ions. The dashed line shows the fit of the model resulting in Na^+/H^+ selectivity in the selective layer of 1.3.

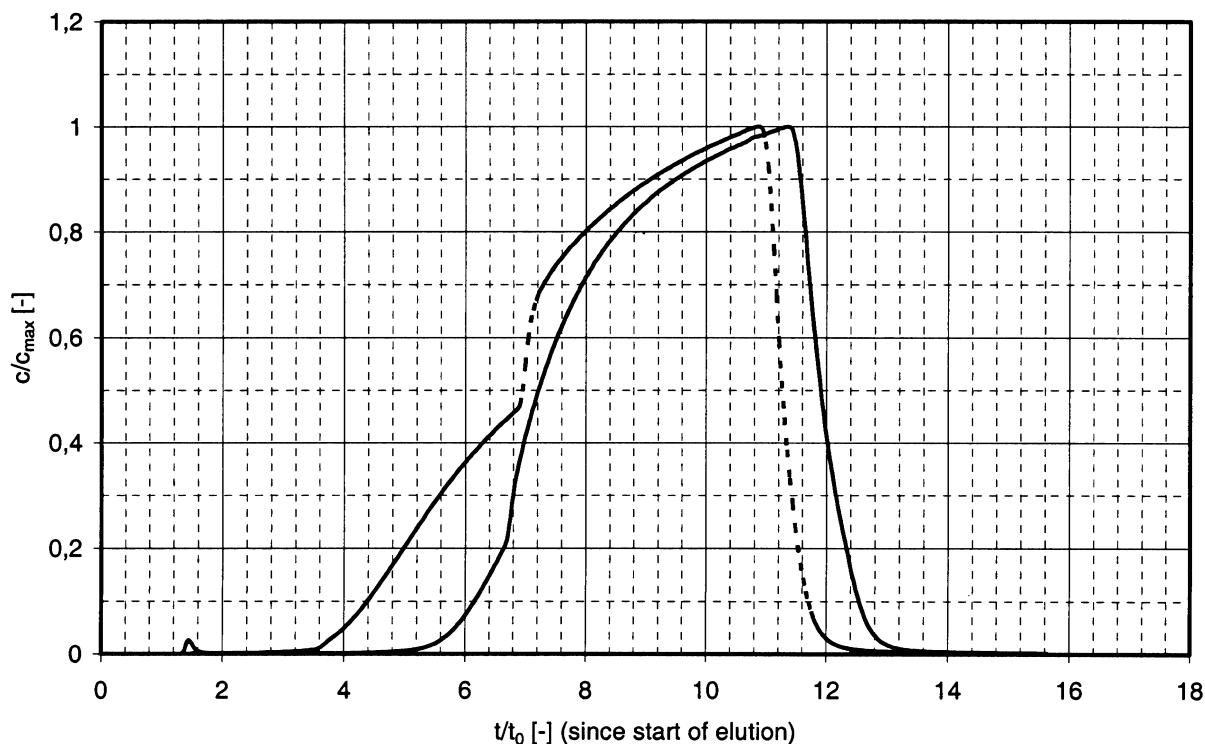


Fig. 7. Influence of salt ions on the retention of compound P by means of adsorption–elution cycles without salt ions (solid line) and with a sodium chloride concentration of 0.85 g/l (dashed line).

difference between adsorption and desorption fronts. The propagation of the axial concentration profiles along the column seen in simulations allows an understanding of the effects involved. In more detail compound P binds to the surface but its maximum resin loading is limited due to the reduced capacity in comparison to hydrogen ions. This does not apply to the sodium ions. Therefore, the sodium ions displace compound P as well as hydrogen ions. These propagate through the column and reduce the solid loading of compound P as can be seen by means of the ion-exchange equilibrium in Fig. 4. Obviously, this leads to a faster elution and to the change in the adsorption front. However, the desorption front is only effected by the displacement by sodium, which results in a reduced column length. The difference in time for the peak maximum is consistent with the remaining bed height available for retardation.

4.4. Simulation of multicomponent systems

In this paper, a three-component mixture was investigated to examine the influence of the side components B and C on the separation. The availability of pure side components is limited, which means that the amounts are too small to measure their single component ion-exchange equilibrium. Instead, pulse experiments were used to measure the retention time and separation factors with respect to compound P (see Fig. 9). Furthermore, the same specific resin capacity for all three components is assumed. The obtained separation factors are 1.28 for compound B and 0.94 for compound C with respect to compound P.

Fig. 10 shows the comparison of experimental and calculated multicomponent adsorption–elution cycles as dimensionless concentrations (based on the total feed concentration) versus the dimensionless time

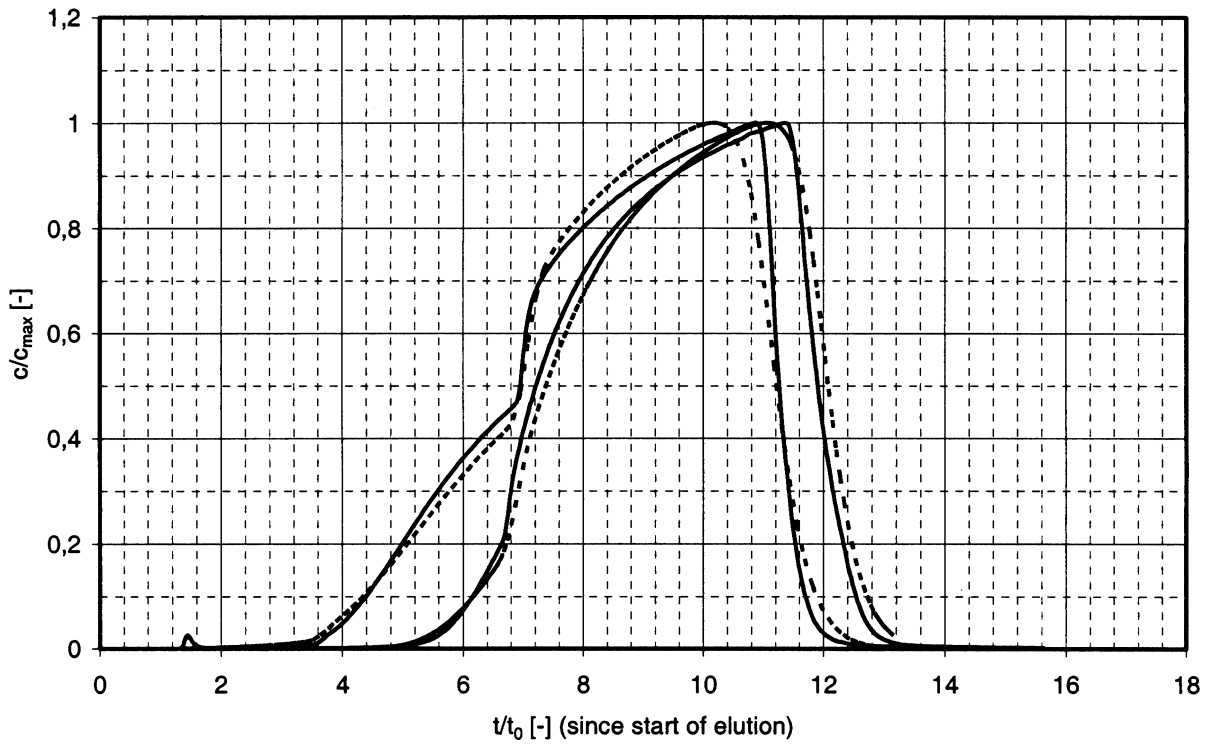


Fig. 8. Experimental (solid lines) and theoretically predicted (dashed lines) elution profiles with and without sodium chloride.

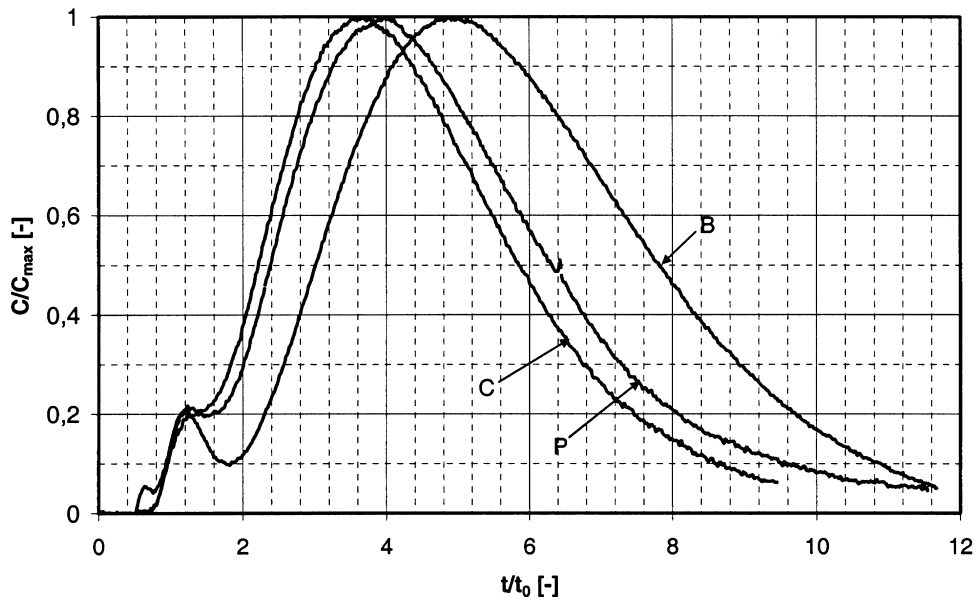


Fig. 9. Pulse experiments for all three components used for determination of the specific selectivity. The pulse experiments are carried out in a small column with 1.6 cm I.D and 3 cm bed height. Isocratic elution in HCl solution of 40 mmol/l is used.

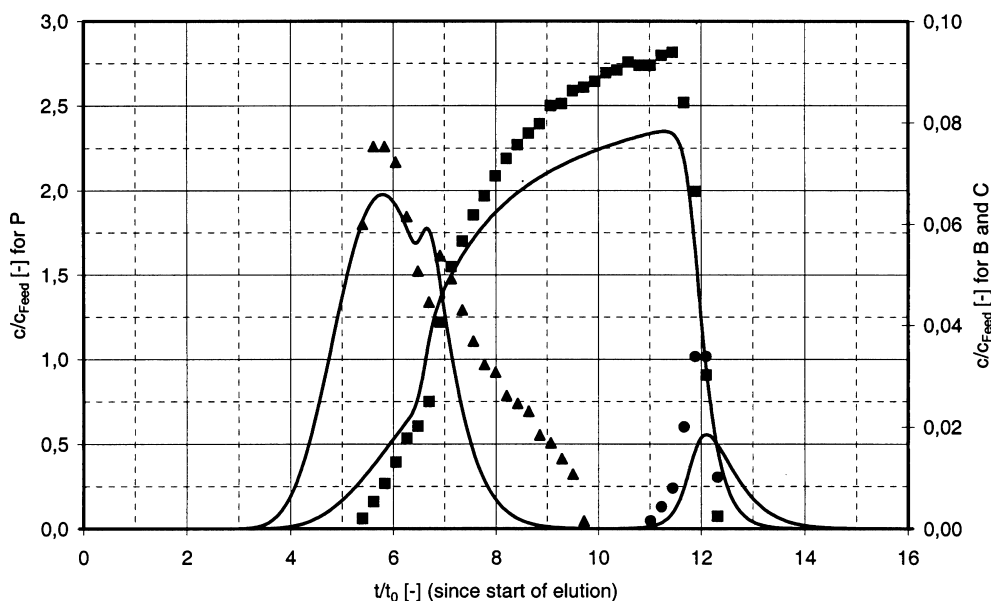


Fig. 10. Experimental (markers) and simulated (solid lines) elution profiles for a three-component system of C (triangles), P (squares) and B (dots) as dimensionless concentrations based on the total feed concentration versus dimensionless time based on the dead volume time.

(based on the dead volume time). As different column loadings at constant feed concentrations result in different durations for the column loading step the time is reset to zero at the start of the elution.

The experimental profile shows the characteristic elution profile for compound P as seen before in single component experiments. The sharp bend in the curve results from the stepwise elution. Solutes eluted by the third elution step move faster through the column and overload the peak eluted by elution step 2. In contrast, the profile shapes of the side components are totally different. Compound B shows the strongest retention and is located in the desorption front of compound P. Its profile is determined by the third and final elution step and gives a Gaussian peak. For compound C a double peak is observed that will be discussed in more detail later.

The calculated adsorption–elution cycles show that the model is able to reproduce the profile shapes in good agreement. Also, the double peak observed for compound C is predicted well. It is noteworthy that the model is able to predict the separation between C and P as seen in experiments though the

separation factor is very small. However, differences in the maximum concentrations remain.

To provide a better insight into the interactions between the components, axial concentration profiles were calculated by interrupting the simulation at discrete time steps. Fig. 11 shows the obtained concentration profiles at the end of the loading step. The concentration of compound C exceeds its feed concentration by more than 300% showing a displacement by compound P. This effect results from a higher feed concentration and a stronger affinity to the resin of compound P. For that reason the double peak can be explained by a combination of displacement by the main component and by formation of peaks by the elution gradient. On the contrary, compound B has a higher selectivity but smaller concentration. Therefore, it is not able to displace compound P but shows a tag-along effect, which has been described in more detail by Guiochon et al. [22]. During the elution the profiles were maintained. The first compound to be desorbed from the resin, compound B, was eluted first but it cannot pass compound P because of its higher selectivity. This means that its band profile is always attached to the

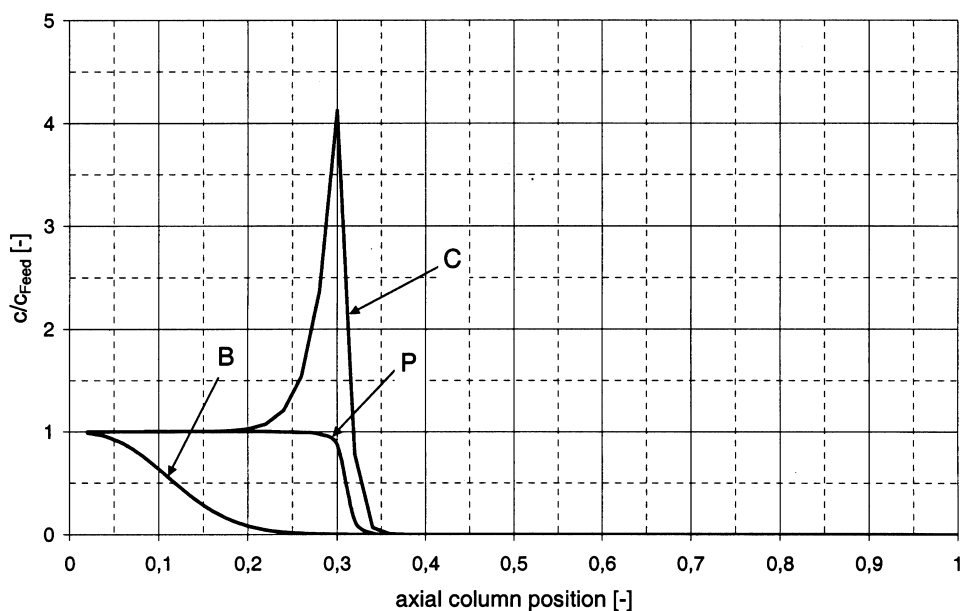


Fig. 11. Axial concentration profiles along the column length after the end of the loading step. Concentrations are based on the specific feed concentrations.

one of compound P. As a consequence, the elution step cannot improve the separation significantly. The same principle applies to the separation of P and C.

The formation of elution peaks and therewith the separation is mostly due to the loading step and the displacement effects observed in this study. This can be seen by calculations of adsorption–elution cycles with different column loadings. As a result, the column was overloaded in terms of feed volume at constant feed concentrations and constant side component fractions of 5% each. The column was loaded to 4%, 20% and 50% of the total specific capacity of compound P (results are shown in Fig. 12). It is interesting to see that the retention time of compound C remains almost constant and shifts only slightly to shorter times. The time needed to elute is given by the remaining column length and the ion-exchange equilibrium in the presence of the eluent. As the length of the unloaded column decreases with increasing volume overload, a small change in time is mandatory. The same principle applies to the adsorption front of compound P. However, the time needed to completely elute the column is a function of the injected amount. Therefore, the peak of compound P starts from a nearly constant adsorption

front and builds up by shifting the desorption front to higher times. As described before the peak of compound B depends on the elution of compound P and therefore elutes later. Due to the displacement the two side components are separated from each other and the overlapping region is reduced. For that reason bigger fractions of pure P can be obtained.

5. Conclusions

This paper introduced a model for the calculation of multicomponent systems in non-linear ion-exchange chromatography. The theory is based on a discrete distribution of counter-ions in the double layer and a mass action equation was applied to consider specific adsorption of the solute counterions to the charged surface. The distinction of both layers was based on the distance from the surface. The model allows neutral components to bind to a charged surface by simultaneous ionization. Theoretically predicted ion-exchange equilibria at neutral pH and two solutions of different elution strength were in good agreement with the measurements. The theory can describe the development of elution

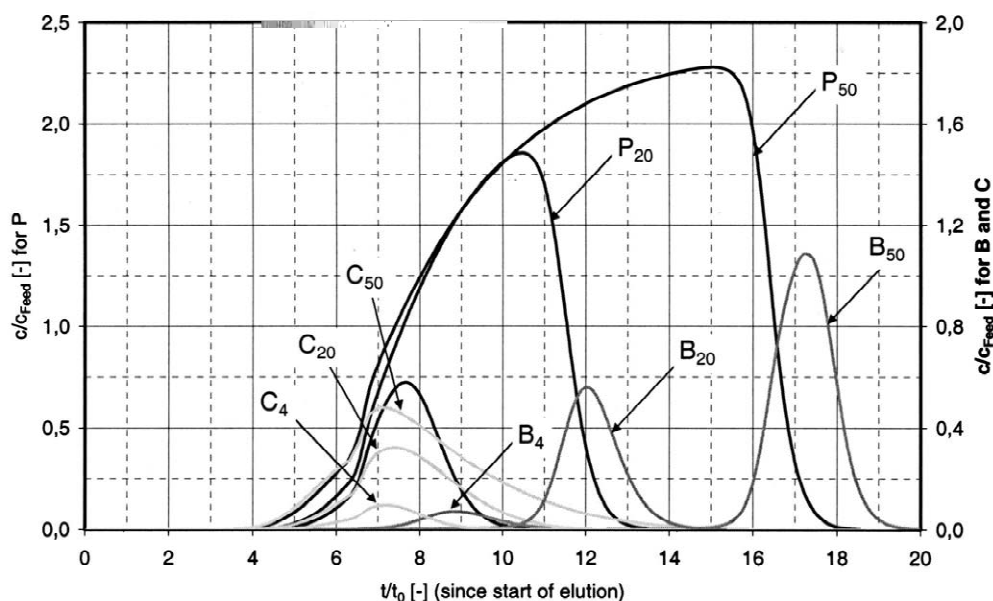


Fig. 12. Calculated adsorption–elution cycles with different column loadings at constant feed concentration and side component fractions of 5% each. The column is loaded to 4%, 20% and 50% (indicated by figures) of the total specific capacity of compound P.

profiles for single components, which are used to show the reliability of the model, and multicomponent systems. The influence of salt ions was considered as competition for the limited number of fixed charges that are supported by comparisons of calculated and measured elution profiles with and without salt ions. Calculations of axial concentration profiles along the column at discrete time steps reveal a strong displacement effect. The separation strongly depends on the displacement, which is a result of the total concentration, column loading and side component fractions. It is furthermore seen that the influence of the elution gradient on the separation is limited.

A generic model has been proposed and experimentally validated for ion-exchange bioseparations. It could be adopted to anion and cation as well as weak and strong ion exchangers. The method, after modifications, is applicable for amino acids with dipolar charge as well as polysaccharides, peptides and proteins with three-dimensional charge distribution. The modifications include a further selectivity in the diffuse layer to describe selectivity

reversals such as observed for amino acids or size exclusion effects in the diffuse layer as the size of proteins usually exceeds the extension of the double layer. Not only the main component but the separation of compounds with similar molecular structure could be described. Furthermore, real process mixtures with contaminants, such as salts, instead of test compounds have been successfully used.

The agreement of the model predictions and experiments is very good and achieves nearly the same accuracy as obtained for the modelling of small molecules, e.g. enantiomers, reached in the last years.

The necessary amounts of process mixtures (not pure components) and laboratory efforts are feasible. However, further scale down of the experiments is aimed at.

Knowledge of the separation mechanisms has increased. Therefore, the general design concepts for ion-exchange could be altered. More importance should be attached to the loading step conditions instead of the sole view on the elution step to improve the separation performance.

6. Nomenclature

c_i	concentration of species i in aqueous phase (mmol/l)	ε	bed voidage
d	diameter (cm)	ε_p	particle porosity
D_{ax}	axial dispersion coefficient (cm ² /s)	ε_0	permittivity of vacuum (F/m)
D_i	diffusivity of species i in aqueous phase (cm ² /s)	ε_r	dielectric constant of the mobile phase
\mathbf{D}_i	effective diffusivity of species i in the stagnant liquid phase in the pores (cm ² /s)	κ	inverse Debye length (l/m)
d_p	resin particle diameter (cm)	ν_i	stoichiometric coefficient of i
f_σ	distribution factor of counter-ions in the double layer	σ_i	steric coefficient of i
J_i	diffusion flux of species i (mmol/cm ² per s)	σ	surface density of fixed charges on the stationary phase (C/m ²)
L	column length (cm)	τ	tortuosity factor
q_i	concentration of species i in solid phase (mol/l)	$\phi(x)$	electrostatical potential in the double layer at a point x from the surface (V)
q_{total}	total exchange capacity of the resin (mol/l)	ϕ_0	electrostatical potential of the surface relative to the bulk of the electrolyte (V)
r	radial coordinate along the particle (cm)	ϕ	electrical potential in the fluid phase (V)
R	gas constant [J/(mol K)]	Superscripts	
t	time (s)	0	in aqueous solution
t_0	column dead time (s)	i	in resin phase
T	temperature (K)	f	feed solution
u	interstitial velocity (cm/s)	s	selective layer
x	axial coordinate along the bed (cm)	d	diffuse layer
X_i	mole fraction of i in the aqueous phase	Subscripts	
Y_i	mole fraction of i in the solid phase	p	particle
z	charge	total	sum of all contributing species
Greek letters		max	maximum value
α_{ij}	selectivity of ion i with respect to ion j		

Acknowledgements

This work was supported by Bayer Technology Services, Process Technology, Leverkusen, Germany, and Bayer Health Care, Biotechnology, Wuppertal, Germany, which provided us with the test

substances, resins as well as laboratory and expert support. The authors would like to thank Dr E. Dikow for his extraordinary mathematical support, Dr R. Wagner for the adsorbent properties support and Drs G. Gutbrod and O. Lockhoff (all Bayer AG) for their physical properties and molecular modelling expertise.

References

- [1] H.S. Thompson, J. R. Agric. Soc. Engl. 11 (1850) 68.
- [2] F.G. Helfferich, Ion Exchange, McGraw-Hill, New York, 1962.
- [3] S. Mattson, Soil Sci. 28 (1929) 179.
- [4] H. Liu, F.F. Cantwell, Anal. Chem. 63 (1991) 993.
- [5] H. Liu, F.F. Cantwell, Anal. Chem. 63 (1991) 2032.
- [6] J. Stahlberg, Anal. Chem. 66 (1994) 440.
- [7] A. Hasnat, V.A. Juvekar, AIChE J. 72 (1996) 161.
- [8] A.L. Myers, S. Byington, in: A.E. Rodrigues (Ed.), Ion Exchange: Science and Technology, Martinus Nijhoff, Dordrecht, 1986, p. 119.
- [9] M.S. Saunders, G. Carta, J.B. Vierow, AIChE J. 35 (1989) 53.
- [10] S.R. Dye, G. Carta, J.P.I. DeCarli, Ind. Eng. Chem. Res. 29 (1990) 849.
- [11] I.L. Jones, G. Carta, Ind. Eng. Chem. Res. 32 (1993) 107.
- [12] S. Melis, G. Cao, M. Morbidelli, Ind. Eng. Chem. Res. 34 (1995) 3916.
- [13] S. Melis, M. Morbidelli, J. Markos, G. Cao, Ind. Eng. Chem. Res. 35 (1996) 3629.
- [14] J.A. Wesselingh, R. Krishna, Mass Transfer, Horwood, New York, 1990.
- [15] Q. Yu, J. Yang, N.-H.L. Wang, React. Polym., Ion Exchangers, Sorbents 6 (1987) 33.
- [16] D. Voet, J.G. Voet, Biochemie, VCH, Weinheim, 1994.
- [17] W.R. Melander, Z. El Rassi, C. Horváth, J. Chromatogr. 469 (1989) 3.
- [18] C.M. Roth, A.M. Lenhoff, Langmuir 9 (1993) 962.
- [19] C.M. Roth, K.K. Unger, A.M. Lenhoff, J. Chromatogr. A 726 (1996) 45.
- [20] S. Cramer, C.A. Brooks, AIChE J. 38 (1992) 1969.
- [21] S. Bouhallab, G. Henry, E. Boschetti, J. Chromatogr. A 724 (1996) 137.
- [22] G. Guiochon, S. Golshan-Shirazi, A.M. Katti, Fundamentals of Preparative and Nonlinear Chromatography, Academic Press, Boston, 1994.
- [23] S.F. Chung, C.Y. Wen, AIChE J. 14 (1968) 857.
- [24] F.G. Helfferich, J. Phys. Chem. 69 (1965) 1178.
- [25] W. Nernst, Z. Phys. Chem. 2 (1888) 613.
- [26] Y.-L. Hwang, F.G. Helfferich, React. Polym. 5 (1987) 237.
- [27] R.A. Robinson, R.M. Stokes, Electrolyte Solutions, Butterworths Scientific Publications, London, 1959.
- [28] A. Polson, J. Phys. Colloidal Chem. 54 (1950) 649.
- [29] C.M. Kim, J.H. Kang, H. Moon, Korean J. Chem. Eng. 12 (1995) 72.
- [30] C.N. Satterfield, Mass Transfer in Heterogeneous Catalysis, MIT Press, Cambridge, MA, 1970.
- [31] J.N. Israelachvili, Intermolecular and Surface Forces, Academic Press, London, 1991.